

Estimate of equilibration times of quantum correlation functions in the thermodynamic limit based on Lanczos coefficients

Jiaozhi Wang ,¹ Merlin Füllgraf ,¹ and Jochen Gemmer ,¹

¹*Department of Mathematics/Computer Science/Physics,
University of Osnabrück, D-49076 Osnabrück, Germany*

(Dated: July 4, 2025)

We study the equilibration times T_{eq} of local observables in quantum chaotic systems by considering their autocorrelation functions. Based on the recursion method, we suggest a scheme to estimate T_{eq} from the corresponding Lanczos coefficients that is expected to hold in the thermodynamic limit. We numerically find that if the observable eventually shows smoothly growing Lanczos coefficients, a finite number of the former is sufficient for a reasonable estimate of the equilibration time. This implies that equilibration occurs on a realistic time scale much shorter than the life of the universe. The numerical findings are further supported by analytical arguments.

Introduction. Whether and how a quantum many-body system approaches equilibrium has long been an important question. It has attracted great attention, both theoretically [1–10] and experimentally [11–15].

Over the past few decades, substantial progress has been made, thanks to the (re)introduction and development of concepts like typicality and the eigenstate thermalization hypothesis (ETH). The ETH explains eventual thermalization of non-integrable systems after sufficiently long times by postulating a particular structure of matrix elements of the observable in the eigenbasis of the Hamiltonian [16–18]. However, it fails to address the question why for physical systems equilibration happens on a conceivable time scale, much shorter than the age of the universe—a question that remains open and actively debated. Analytical efforts have primarily focused on establishing bounds for equilibration time. In recent years, several bounds have been rigorously derived [2, 7, 19–23], significantly improving our understanding of the timescale of equilibration. However, in the existing analytical studies, the general assumptions underlying the approaches are often violated in typical physical settings, see e.g. Refs. [24, 25]. Consequently, questions arise considering the relevance of such bounds to the equilibration in real systems.

In addition to the analytical work, the problem has also been studied numerically [26]. Due to limitations on the system size that are numerically accessible, the equilibration timescale in the thermodynamic limit remains an open question.

In our recent work [5], we tackled this problem employing an approach based on the so-called recursion method. In this work we elaborate on a direct scheme, based on smoothly growing Lanczos coefficients, to infer the equilibration time in the thermodynamic limit. Numerically, we find that if the Lanczos coefficients exhibit such a behaviour, our method converges quickly, indicating a reasonable and cheap estimate, once the first several Lanczos coefficients are taken into account. Furthermore, we present analytical arguments supporting our numerical

findings and suggesting the typicality of finite equilibration times in real physical systems.

Framework. Given an observable \mathcal{O} and a Hamiltonian H we are interested in the autocorrelation

$$\mathcal{C}(t) = \frac{\text{Tr}[\mathcal{O}(t)\mathcal{O}]}{\text{Tr}[\mathcal{O}^2]}, \quad (1)$$

where $\mathcal{O}(t) = e^{iHt}\mathcal{O}e^{-iHt}$. In our paper, we focus on the following definition of equilibration time [10]

$$T_{\text{eq}} := \int_0^\infty |\mathcal{C}(t) - \mathcal{C}(\infty)|^2 dt, \quad (2)$$

where $\mathcal{C}(\infty) = \lim_{T \rightarrow \infty} \frac{1}{T} \int_0^T \mathcal{C}(t) dt$. Assuming $\mathcal{C}(\infty) = 0$, T_{eq} becomes

$$T_{\text{eq}} = \int_0^\infty \mathcal{C}^2(t) dt. \quad (3)$$

The equilibration time T_{eq} can be interpreted as the area under the curve of $\mathcal{C}^2(t)$. To illustrate the physical meaning of T_{eq} defined above, consider the simple example $\mathcal{C}(t) = e^{-\Gamma t} \cos(\omega t)$, for which $T_{\text{eq}} = \frac{1}{4\Gamma} + \frac{\Gamma}{4(\Gamma^2 + \omega^2)} \sim \frac{1}{\Gamma}$. Without the square in Eq. (3), the integral $\int_0^\infty \mathcal{C}(t) dt = \frac{\Gamma}{\Gamma^2 + \omega^2}$ would fail to capture the relevant timescale of thermalization, e.g., in case of rapid oscillation $\omega \gg \Gamma$.

To introduce the general framework, it is convenient to switch to the Hilbert space of operators, also Liouville space, and denote its elements \mathcal{O} by states $|\mathcal{O}\rangle$. This space is equipped with an inner product $\langle \mathcal{O}_m | \mathcal{O}_n \rangle = \text{Tr}[\mathcal{O}_m^\dagger \mathcal{O}_n] / \text{Tr}[1]$, which defines a norm via $\|\mathcal{O}\| = \sqrt{\langle \mathcal{O} | \mathcal{O} \rangle}$. The Liouvillian superoperator is defined by $\mathcal{L}|\mathcal{O}\rangle = |[H, \mathcal{O}] \rangle$, where H denotes the Hamiltonian of the system, and propagates a state $|\mathcal{O}\rangle$ in time, such that an autocorrelation function (at infinite temperature) can be written as

$$\mathcal{C}(t) = \langle \mathcal{O} | e^{i\mathcal{L}t} | \mathcal{O} \rangle. \quad (4)$$

Starting from an initial “seed” \mathcal{O} , a tridiagonal representation of \mathcal{L} can be obtained using the Lanczos algorithm. From a normalized initial state $|\mathcal{O}_0\rangle \propto |\mathcal{O}\rangle$,

i.e., $(\mathcal{O}_0|\mathcal{O}_0) = 1$, we set $b_1 = \|\mathcal{L}|\mathcal{O}_0)\|$ as well as $|\mathcal{O}_1) = \mathcal{L}|\mathcal{O}_0)/b_1$. Then, we iteratively compute

$$\begin{aligned} |\tilde{\mathcal{O}}_n) &= \mathcal{L}|\mathcal{O}_{n-1}) - b_{n-1}|\mathcal{O}_{n-2}), \\ b_n &= \|\tilde{\mathcal{O}}_n\|, \\ |\mathcal{O}_n) &= |\tilde{\mathcal{O}}_n)/b_n. \end{aligned} \quad (5)$$

The tridiagonal representation of \mathcal{L} in the Krylov basis $\{|\mathcal{O}_n)\}$ results as

$$\mathcal{L}_{mn} = (\mathcal{O}_m|\mathcal{L}|\mathcal{O}_n) = \delta_{m,n+1}b_n + \delta_{m,n-1}b_m, \quad (6)$$

where the coefficients b_n are real and positive numbers, referred to as Lanczos coefficients. The (infinite) set of Lanczos coefficients uniquely determines the autocorrelation function and vice versa. Their iterative computation is an elementary part of the recursion method. Note that it is possible to calculate a certain number of b_n (practically in the lower two digit regime) even for infinitely large systems, i.e., in the thermodynamic limit, if the Hamiltonian and the observable are local. In the remainder of the paper at hand we address this scenario. Furthermore, in Mori formalism [27, 28], the Lanczos coefficients b_n are directly related to the Laplace transform of the respective autocorrelation function via a continued fraction representation of form

$$\mathcal{F}(s) = \int_0^\infty e^{ts} \mathcal{C}(t) dt = \frac{1}{s + \frac{b_1^2}{s + \frac{b_2^2}{s + \dots}}}, \quad (7)$$

see also [29]. From Eq. (7), we infer that the infinite-time integral of $\mathcal{C}(t)$ is solely determined by the Lanczos coefficients as

$$\mathcal{F}(0) = \int_0^\infty \mathcal{C}(t) dt = \frac{1}{b_1} \prod_{n=1}^\infty \left(\frac{b_n}{b_{n+1}} \right)^{(-1)^n}. \quad (8)$$

Consequently, returning to the original question, the equilibration time T_{eq} defined in Eq. (3) may be computed by virtue of the Lanczos coefficients related to the autocorrelation function $\mathcal{C}^2(t)$, denoted by B_n .

To study the B_N , we consider a product space spanned by $\{|mn)\} := \{|\mathcal{O}_m)\otimes|\mathcal{O}_n)\}$, and a Liouvillian superoperator $\mathcal{L}' = \mathcal{L} \otimes \mathbb{1} + \mathbb{1} \otimes \mathcal{L}$. In this setting the observable corresponding to $\mathcal{C}^2(t)$ may be understood as $\mathcal{O}' = \mathcal{O} \otimes \mathcal{O}$, such that

$$\mathcal{C}^2(t) = (\mathcal{O}'|e^{i\mathcal{L}'t}|\mathcal{O}') = (\mathcal{O}|e^{i\mathcal{L}t}|\mathcal{O})(\mathcal{O}|e^{i\mathcal{L}t}|\mathcal{O}), \quad (9)$$

relating the setting to the simple case as in Eq. (4). The Lanczos coefficient B_N is calculated using \mathcal{L}' and a “seed” operator in the product space $|\mathcal{Q}_0) = |00)$. Specifically, we determine $B_1 = \|\mathcal{L}'|\mathcal{Q}_0)\|$ and set $|\tilde{\mathcal{Q}}_1) = \mathcal{L}'|\mathcal{Q}_0)$ and again follow the Lanczos scheme

$$\begin{aligned} |\tilde{\mathcal{Q}}_N) &= \mathcal{L}'|\mathcal{Q}_{N-1}) - B_{N-1}|\mathcal{Q}_{N-2}), \\ B_N &= \|\tilde{\mathcal{Q}}_N\|, \\ |\mathcal{Q}_N) &= |\tilde{\mathcal{Q}}_N)/B_N. \end{aligned} \quad (10)$$

Given the b_n , the B_N can be calculated straightforwardly using Eq. (10), e.g.,

$$\begin{aligned} |\tilde{\mathcal{Q}}_1) &= b_1(|10) + |01)), \\ B_1 &= \sqrt{2}b_1, \dots, B_2 = \sqrt{2b_1^2 + b_2^2}, \dots, \end{aligned} \quad (11)$$

which indicates that B_N are unambiguously determined by $b_{n(n \leq N)}$. With the Lanczos coefficients B_N we can eventually formulate the equilibration time T_{eq} similarly to Eq. (8) as

$$T_{\text{eq}} \equiv \int_0^\infty \mathcal{C}^2(t) dt = \frac{1}{B_1} \prod_{N=1}^\infty \left(\frac{B_N}{B_{N+1}} \right)^{(-1)^N}. \quad (12)$$

Crucially, the scheme described in Eq. (10) is considerably simpler than the original Lanczos algorithm for $\mathcal{C}(t)$, Eq. (5), once by virtue of the coefficients b_n the operators \mathcal{L}_{mn} are known. This is our first main result of the paper.

In practice, only the first several b_n are easily numerically accessible. Let n_{max} denotes the number of feasible b_n . From these b_n we calculate the first $B_{N(N \leq R)}$ using the scheme (10), which is applicable up to $R \leq n_{\text{max}}$. For convenience in the following discussion, let us rewrite Eq. (12) as

$$T_{\text{eq}} = \begin{cases} \frac{1}{p_R B_R} \prod_{M=1}^{\frac{R}{2}} \frac{B_{2M}^2}{B_{2M-1}^2} & , \text{even } R \\ \frac{p_R}{B_R} \prod_{M=1}^{\frac{R-1}{2}} \frac{B_{2M}^2}{B_{2M-1}^2} & , \text{odd } R \end{cases}, \quad (13)$$

where

$$p_{R+1} = \prod_{M=1}^\infty \left(\frac{B_{R+M}}{B_{R+M+1}} \right)^{(-1)^M}. \quad (14)$$

Now we resort to an assumption that the remaining $B_{N(N > R)}$ grow linearly, $B_N(N > R) = \alpha_R N + \beta_R$. In this case, p_R can be derived analytically (detailed in supplemental material),

$$\tilde{p}_R = \frac{\Gamma(\frac{R}{2} + \frac{\beta_R}{2\alpha_R}) \Gamma(\frac{R}{2} + \frac{\beta_R}{2\alpha_R} + 1)}{\Gamma^2(\frac{R}{2} + \frac{\beta_R}{2\alpha_R} + \frac{1}{2})}. \quad (15)$$

Here, we use a rather simple approach, where α_R and β_R are obtained from a linear extrapolation of the two last exact B_N , i.e., $\alpha_R = B_R - B_{R-1}$ and $\beta_R = R B_{R-1} - (R-1) B_R$. This yields the following estimate:

$$T_{\text{eq}} \simeq T_{\text{eq}}^{\text{rc}} = \begin{cases} \frac{1}{\tilde{p}_R B_R} \prod_{M=1}^{\frac{R}{2}} \frac{B_{2M}^2}{B_{2M-1}^2} & , \text{even } R \\ \frac{\tilde{p}_R}{B_R} \prod_{M=1}^{\frac{R-1}{2}} \frac{B_{2M}^2}{B_{2M-1}^2} & , \text{odd } R \end{cases}. \quad (16)$$

This estimate would be exact if the above extrapolation captured the true B_N precisely. More importantly, it may be still very close, even if the $B_{N(N > R)}$ are not precisely linear but smooth (for a formal definition see

Eq. (22)). This is tantamount to stating that T_{eq} is not very sensitive to the B_N at larger N as long as they are smooth. Fig. S7 in the supplemental material provides an instructive example for $b_N \propto \sqrt{N}$.

At this point a crucial conceptual question arises: Under which conditions will the B_N become eventually smooth? If they do so, this entails a technical question: Is the practically available number of b_n large enough such that R reaches into a regime in which the true B_N are sufficiently smooth?

To address the conceptual question, here we rely on an argument which is presented in detail in the supplemental material: Given a *smooth* profile of the original b_n above some n_s , we approximately find

$$B_N \approx 2b_{N/2} \quad (17)$$

for $N \geq 2n_s$. This means the B_N may inherit smoothness from the b_n . Smoothness of the b_n may, however, be to some extent based on the *operator growth hypothesis* [30]. It states that in infinite chaotic quantum many-body systems the Lanczos coefficients of local operators that have no overlap with any conserved quantity, are asymptotically linear (with logarithmic corrections in one dimension). Thus, as the convergence of $T_{\text{eq}}^{\text{rc}}$ occurs for smooth b_n , the former is generally expected for such local observables in chaotic quantum systems. The answer to the technical question, however, will rely more on the numerical results presented below.

Numerical results. To check our assumptions and main results, as well as to address the technical question stated above, we consider some physical models for which we compute n_{max} Lanczos coefficients per operator. The number n_{max} differs for each model because of the numerical complexity. However, all n_{max} Lanczos coefficients correspond to the respective infinite system. The first model we consider is an Ising ladder,

$$H = H_1 + \lambda H_I + H_2, \quad (18)$$

where

$$H_r = \sum_{\ell=1}^{L/2} h_x \sigma_{r,\ell}^x + h_z \sigma_{r,\ell}^z + J \sigma_{r,\ell}^z \sigma_{r,\ell+1}^z, \\ H_I = \sum_{\ell=1}^{L/2} \sigma_{1,\ell}^z \sigma_{2,\ell}^z. \quad (19)$$

Here $\sigma_{r,\ell+1}^{x,z}$ indicates the Pauli matrix at site (r, ℓ) , where $r = 1, 2$ and $\ell = 1, 2, \dots, L/2$. Here L is chosen to be even. The operator of interest is the energy-difference operator $\mathcal{A}_\Delta = H_1 - H_2$. Parameters are chosen as $h_x = 1.0$, $h_z = 0.5$, $J = 1.0$. For this model we obtain $n_{\text{max}} = 24$ Lanczos coefficients.

As a second model, we study a tilted field Ising (TFI) chain,

$$H = \sum_{\ell=1}^L h_x \sigma_\ell^x + \lambda \sigma_\ell^z + J \sigma_\ell^z \sigma_{\ell+1}^z, \quad (20)$$

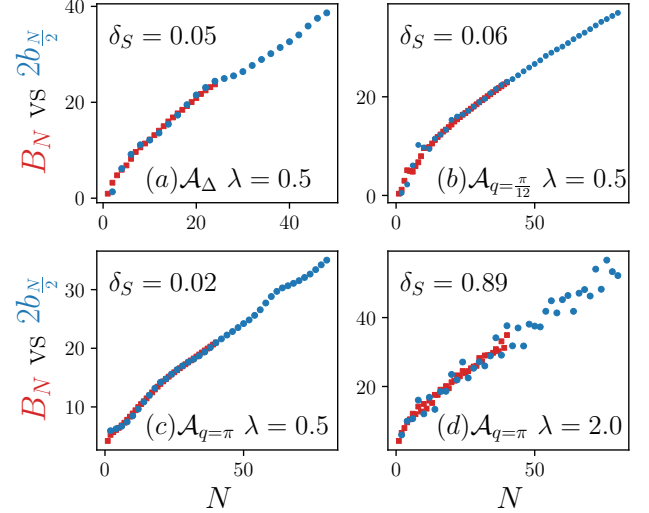


FIG. 1. Lanczos coefficients B_N (red square) related to the autocorrelation function C^2 versus $2b_{N/2}$ (blue dot) with b_n the Lanczos coefficients related to \mathcal{C} , for different models, observables and system parameters. (a): Ising ladder, energy difference operator \mathcal{A}_Δ , $\lambda = 0.5$; and tilted field Ising model, energy density wave operator \mathcal{A}_q for (b): $q = \pi/12$, $\lambda = 0.5$; (c): $q = \pi$, $\lambda = 0.5$ and (d): $q = \pi$, $\lambda = 2.0$. q indicates the wavenumber of the density-wave operator \mathcal{A}_q . δ_S is the smoothness indicator defined in Eq. (22).

where we focus on energy density wave operators $\mathcal{A}_q = \sum_{\ell=1}^L \cos(q\ell) h_\ell$, where h_ℓ indicates the local energy

$$h_\ell = \frac{h_x}{2} (\sigma_\ell^x + \sigma_{\ell+1}^x) + \frac{\lambda}{2} (\sigma_\ell^z + \sigma_{\ell+1}^z) + J \sigma_\ell^z \sigma_{\ell+1}^z. \quad (21)$$

In the numerical investigation, we fix $h_x = 1.05$, $J = 1.0$. Two different wave numbers are considered here, $q = \pi$ and $q = \pi/12$. Here, for both observables we obtain $n_{\text{max}} = 40$ Lanczos coefficients.

As a start, we show some examples of Lanczos coefficients in Fig. 1. To characterize the smoothness of b_n , we introduce a “smoothened” version of the b_n , given by $\tilde{b}_n := \frac{1}{4}b_{n-1} + \frac{1}{2}b_n + \frac{1}{4}b_{n+1}$ ($n \geq 2$). The smoothness δ_S is thus defined as

$$\delta_S = \frac{1}{n_{\text{max}} - 2} \sum_{n=2}^{n_{\text{max}}-1} |b_n - \tilde{b}_n|. \quad (22)$$

In [(a)(b)(c)], approximately smooth b_n with a small δ_S are observed, whereas in (d), significant fluctuations in b_n are evident, corresponding to a large δ_S , see Fig. 1.

Moreover, we verify $B_N \approx 2b_{N/2}$, where B_N is computed from the scheme (10). When the original b_n become smooth for growing n (as indicated by a small δ_S), there is a good agreement, as shown in [(a)(b)(c)]. In contrast, if the b_n are not smooth, their non-smooth structure carries over to the B_N , leading to deviations between B_N and $2b_{N/2}$. This is in accord with the principles stated

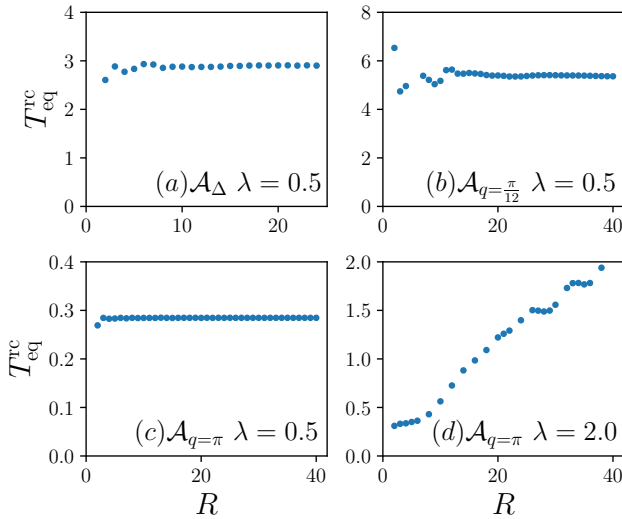


FIG. 2. Equilibration time $T_{\text{eq}}^{\text{rc}}$ (given in Eq. (16)) for different numbers R of included Lanczos coefficients, for different models, observables and system parameters. (a): Ising ladder, energy difference operator \mathcal{A}_Δ , $\lambda = 0.5$; and tilted field Ising model, energy density wave operator \mathcal{A}_q for (b): $q = \pi/12$, $\lambda = 0.5$; (c): $q = \pi$, $\lambda = 0.5$ and (d): $q = \pi$, $\lambda = 2.0$.

around Eq. (17), and detailed in the supplemental material.

In Fig. 2 we exemplary show our estimation of $T_{\text{eq}}^{\text{rc}}$ for varying R for the cases [(a)-(d)] discussed in Fig. 1. In the cases of *smooth* Lanczos coefficients, here [(a)-(c)] as indicated by small δ_S , $T_{\text{eq}}^{\text{rc}}$ only varies slightly with respect to R , for $R \gtrsim 5$. This observation suggests that the first several Lanczos coefficients are sufficient to obtain a reasonable estimate of T_{eq} . Conversely, in the scenario (d), where the Lanczos coefficients are not smooth (large δ_S), the quantity $T_{\text{eq}}^{\text{rc}}$ does not converge, indicating that an accurate result for T_{eq} might not yet have been reached.

Strictly speaking, an apparent convergence of $T_{\text{eq}}^{\text{rc}}$ at finite R does not yet warrant the correctness of the estimate. Thus we compare $T_{\text{eq}}^{\text{rc}}$ with results from direct simulations of the autocorrelation function. More precisely, we study the pendant of the equilibration time, see Eq. (3), given by $T_{\text{eq}}^{\text{typ}} := \int_0^{T_c} \mathcal{C}^2(t) dt$, with appropriate T_c , for details see [31]. Here we consider a finite system size $L = 24$, where $\mathcal{C}(t)$ is calculated using dynamical quantum typicality [32]. (Non-systematic checking indicates that for all considered cases $T_{\text{eq}}^{\text{typ}}$ does not strongly depend on L for $L \geq 24$.)

If δ_S is small ($\delta_S < 0.2$), as shown by open dots in Fig. 3, we observe $T_{\text{eq}}^{\text{rc}} \approx T_{\text{eq}}^{\text{typ}}$, which indicates the high accuracy of our estimation in this regime. In case of larger δ_S ($\delta_S \geq 0.2$), $T_{\text{eq}}^{\text{rc}}$ begins to deviate from $T_{\text{eq}}^{\text{typ}}$. This suggests that once the Lanczos coefficients are smooth, our method tends to converge with good accuracy. For more detailed data on the relation of smooth-

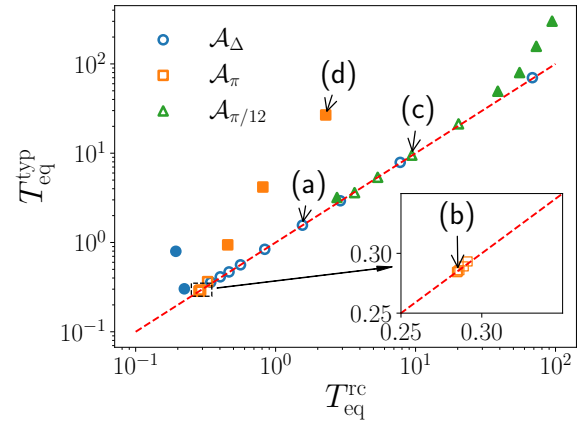


FIG. 3. Comparison between the equilibration time estimated using the recursion method $T_{\text{eq}}^{\text{rc}}$ (Eq. (16)), and that obtained from exact dynamics $T_{\text{eq}}^{\text{typ}}$ for different observables and λ ($\lambda \in [0.1, 2.0]$ for \mathcal{A}_π and $\mathcal{A}_{\pi/12}$, and $\lambda \in [0.1, 4.0]$ for \mathcal{A}_Δ). (a)-(d) refer to the corresponding cases illustrated in Figs. 1 and 2.

ness of Lanczos coefficients and the and the accuracy of our approach see Fig. S6 in the supplemental material. In the End Matter, we examine the spin density wave operator in the Heisenberg XXZ model and also find that our approach yields good accuracy when the b_n grow in a smooth fashion.

Based on these findings we believe our methods does converge for a very wide range of autocorrelation functions in fully chaotic systems as a multitude of numerical studies reveal the respective Lanczos coefficients b_n to be smooth early on, see e.g. [29, 30, 33, 34]. It appears that smoothness of Lanczos coefficients and chaos are interlinked. For the average gap ratios $\langle r \rangle$ [35] corresponding to the Hamiltonians of our four main examples, illustrated in Figs. 1 and 2 we find (for $L = 18$) (a): $\langle r \rangle = 0.53$, (b)(c): $\langle r \rangle = 0.53$, (d): $\langle r \rangle = 0.46$. Note that full chaoticity is characterized by $\langle r \rangle \approx 0.53$. Hence the case with poor convergence, (d), is also the least chaotic case.

Conclusion and Outlook. In this paper, based on the recursion method, we suggest a scheme to estimate the equilibration times of local observables, by making use of the corresponding Lanczos coefficients. We numerically find that such estimations converge quickly when the first several Lanczos coefficients are taken into account, provided that the observable eventually features smoothly growing Lanczos coefficients. It implies that the first several Lanczos coefficients are sufficient for a reasonable estimate of T_{eq} in the thermodynamic limit. Our numerical findings are further supported by analytical arguments.

A natural future direction is to apply our approach to other types of systems, including the Fermi Hubbard model, models with disorder as well as higher dimensional systems. It is also interesting to extend our frame-

work to time-dependent systems, or, Floquet systems, to estimate the equilibration time towards time-dependent steady states. Benchmarking the results against those from large-scale systems using Density Matrix Renormalization Group (DMRG) calculations could also provide important insights to further assess the accuracy of the approach.

Outline of supplemental material. In the supplemental material we argue that for smooth Lanczos coefficients the formula $B_N \approx 2b_{N/2}$ for the Lanczos coefficients of the squared dynamics holds approximately. Based on the observation that the Krylov vectors $|Q_n\rangle$ subject to the scheme in Eq. (10) are primarily located at the outmost counterdiagonal of the product space $\{|n\rangle \otimes |m\rangle\}$, the argument is laid out in the framework of a stochastic process imposed by \mathcal{L} .

Acknowledgement. This work has been funded by the Deutsche Forschungsgemeinschaft (DFG), under Grant No. 531128043, as well as under Grant No. 397107022, No. 397067869, and No. 397082825 within the DFG Research Unit FOR 2692, under Grant No. 355031190. Additionally, we greatly acknowledge computing time on the HPC3 at the University of Osnabrück, granted by the DFG, under Grant No. 456666331.

[1] C. Gogolin and J. Eisert, *Equilibration, thermalisation, and the emergence of statistical mechanics in closed quantum systems*, *Reports on Progress in Physics* **79**, 056001 (2016).

[2] L. P. García-Pintos, N. Linden, A. S. L. Malabarba, A. J. Short, and A. Winter, *Equilibration time scales of physically relevant observables*, *Phys. Rev. X* **7**, 031027 (2017).

[3] S. Goldstein, T. Hara, and H. Tasaki, *Extremely quick thermalization in a macroscopic quantum system for a typical nonequilibrium subspace*, *New Journal of Physics* **17**, 045002 (2015).

[4] M. Kastner, *Diverging equilibration times in long-range quantum spin models*, *Phys. Rev. Lett.* **106**, 130601 (2011).

[5] C. Bartsch, A. Dymarsky, M. H. Lamann, J. Wang, R. Steinigeweg, and J. Gemmer, *Estimation of equilibration time scales from nested fraction approximations*, *Phys. Rev. E* **110**, 024126 (2024).

[6] P. Reimann, *Typical fast thermalization processes in closed many-body systems*, *Nature Communications* **7**, 10821 (2016).

[7] A. S. L. Malabarba, L. P. García-Pintos, N. Linden, T. C. Farrelly, and A. J. Short, *Quantum systems equilibrate rapidly for most observables*, *Phys. Rev. E* **90**, 012121 (2014).

[8] H. Wilming, M. Goihl, I. Roth, and J. Eisert, *Entanglement-ergodic quantum systems equilibrate exponentially well*, *Phys. Rev. Lett.* **123**, 200604 (2019).

[9] S. Goldstein, T. Hara, and H. Tasaki, *Time scales in the approach to equilibrium of macroscopic quantum systems*, *Phys. Rev. Lett.* **111**, 140401 (2013).

[10] A. M. Alhambra, J. Riddell, and L. P. García-Pintos, *Time evolution of correlation functions in quantum many-body systems*, *Phys. Rev. Lett.* **124**, 110605 (2020).

[11] R. Geiger, T. Langen, I. Mazets, and J. Schmiedmayer, *Local relaxation and light-cone-like propagation of correlations in a trapped one-dimensional bose gas*, *New Journal of Physics* **16**, 053034 (2014).

[12] T. Langen, R. Geiger, M. Kuhnert, B. Rauer, and J. Schmiedmayer, *Local emergence of thermal correlations in an isolated quantum many-body system*, *Nature Physics* **9**, 640 (2013).

[13] P. Richerme, Z.-X. Gong, A. Lee, C. Senko, J. Smith, M. Foss-Feig, S. Michalakis, A. V. Gorshkov, and C. Monroe, *Non-local propagation of correlations in quantum systems with long-range interactions*, *Nature* **511**, 198 (2014).

[14] S. Trotzky, Y.-A. Chen, A. Flesch, I. P. McCulloch, U. Schollwöck, J. Eisert, and I. Bloch, *Probing the relaxation towards equilibrium in an isolated strongly correlated one-dimensional bose gas*, *Nature physics* **8**, 325 (2012).

[15] P. Jurcevic, B. P. Lanyon, P. Hauke, C. Hempel, P. Zoller, R. Blatt, and C. F. Roos, *Quasiparticle engineering and entanglement propagation in a quantum many-body system*, *Nature* **511**, 202 (2014).

[16] J. M. Deutsch, *Quantum statistical mechanics in a closed system*, *Phys. Rev. A* **43**, 2046 (1991).

[17] M. Srednicki, *Chaos and quantum thermalization*, *Phys. Rev. E* **50**, 888 (1994).

[18] M. Rigol, V. Dunjko, and M. Olshanii, *Thermalization and its mechanism for generic isolated quantum systems*, *Nature* **452**, 854 (2008).

[19] A. J. Short and T. C. Farrelly, *Quantum equilibration in finite time*, *New Journal of Physics* **14**, 013063 (2012).

[20] P. Reimann and M. Kastner, *Equilibration of isolated macroscopic quantum systems*, *New Journal of Physics* **14**, 043020 (2012).

[21] P. Figueroa-Romero, K. Modi, and F. A. Pollock, *Equilibration on average in quantum processes with finite temporal resolution*, *Phys. Rev. E* **102**, 032144 (2020).

[22] A. M. Alhambra, J. Riddell, and L. P. García-Pintos, *Time evolution of correlation functions in quantum many-body systems*, *Phys. Rev. Lett.* **124**, 110605 (2020).

[23] T. R. de Oliveira, C. Charalambous, D. Jonathan, M. Lewenstein, and A. Riera, *Equilibration time scales in closed many-body quantum systems*, *New Journal of Physics* **20**, 033032 (2018).

[24] R. Heveling, L. Knipschild, and J. Gemmer, *Compelling bounds on equilibration times—the issue with fermi’s golden rule*, *Journal of Physics A: Mathematical and Theoretical* **53**, 375303 (2020).

[25] R. Heveling, L. Knipschild, and J. Gemmer, *Comment on “equilibration time scales of physically relevant observables”*, *Phys. Rev. X* **10**, 028001 (2020).

[26] S. Genway, A. F. Ho, and D. K. K. Lee, *Thermalization of local observables in small hubbard lattices*, *Phys. Rev. A* **86**, 023609 (2012).

[27] C. Joslin and C. Gray, *Calculation of transport coefficients using a modified mori formalism*, *Molecular Physics* **58**, 789 (1986).

[28] H. Mori, *Transport, collective motion, and Brownian motion*, *Prog. Theor. Phys.* **33**, 423 (1965).

[29] J. Wang, M. H. Lamann, R. Steinigeweg, and J. Gemmer, *Diffusion constants from the recursion method*, *Phys. Rev. B* **110**, 104413 (2024).

- [30] D. E. Parker, X. Cao, A. Avdoshkin, T. Scaffidi, and E. Altman, *A universal operator growth hypothesis*, *Phys. Rev. X* **9**, 041017 (2019).
- [31] T_c indicates the (sufficiently late) point in time at which the integral is cut off. This is necessary as in finite systems such an expression always diverges. Hence we choose the cutoff time T_c as the time after which $\mathcal{C}^2(t) \leq 0.001$ for all computable times $t \geq T_c$. Further it shall be noted that in practice the value of T_{eq} is not sensible to the choice of T_c . More details are given in the supplemental material.
- [32] C. Bartsch and J. Gemmer, *Dynamical typicality of quantum expectation values*, *Phys. Rev. Lett.* **102**, 110403 (2009).
- [33] R. Heveling, J. Wang, and J. Gemmer, *Numerically probing the universal operator growth hypothesis*, *Phys. Rev. E* **106**, 014152 (2022).
- [34] F. Uskov and O. Lychkovskiy, *Quantum dynamics in one and two dimensions via the recursion method*, *Phys. Rev. B* **109**, L140301 (2024).
- [35] V. Oganesyan and D. A. Huse, *Localization of interacting fermions at high temperature*, *Phys. Rev. B* **75**, 155111 (2007).
- [36] O. Penrose, *Foundations of statistical mechanics: A deductive treatment* (Pergamon Press, 1969).

End Matter

In the End Matter, we present numerical results for spin density wave operators in the Heisenberg XXZ model. The Hamiltonian reads

$$H = \sum_{\ell=1}^L J(s_{\ell}^x s_{\ell+1}^x + s_{\ell}^y s_{\ell+1}^y + \lambda s_{\ell}^z s_{\ell+1}^z + \Delta' s_{\ell}^z s_{\ell+2}^z), \quad (23)$$

where $s_{\ell}^{x,y,z} = \frac{1}{2}\sigma_{\ell}^{x,y,z}$ indicates the spin operator at site ℓ . Parameters are chosen as $J = 1.0, \Delta' = 0.5$. Here we consider the spin density wave operator

$$\mathcal{A}_q^S = \sum_{\ell=1}^L \cos(q\ell) s_{\ell}^z, \quad (24)$$

where q indicates the wave number and we focus on $q = \pi$ and $q = \pi/14$. The results are shown in Figs. 4, 5 and 6, analogue to Figs. 1, 2 and 3 in the main text. For both observables we obtain $n_{\max} = 17$ Lanczos coefficients.

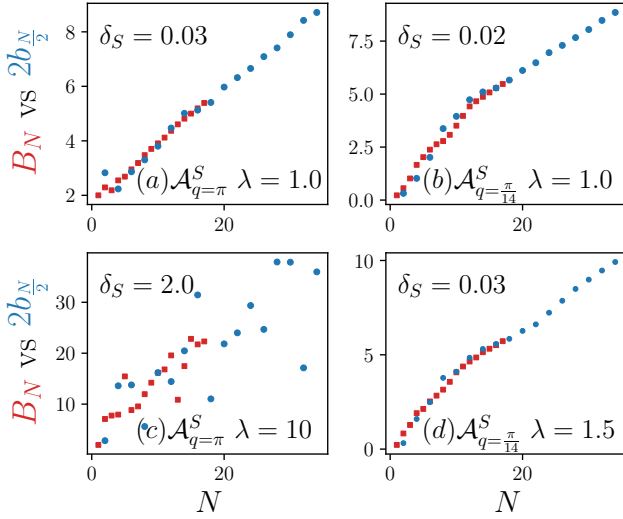


FIG. 4. Lanczos coefficients B_N (red square) related to the autocorrelation function \mathcal{C}^2 versus $2b_{N/2}$ (blue dot) with b_n the Lanczos coefficients related to \mathcal{C} , for the spin density wave operators in XXZ model. The results are shown for different λ and wave number q . (a): $q = \pi, \lambda = 1.0$; (b) $q = \pi/14, \lambda = 1.0$; (c): $q = \pi, \lambda = 10.0$ and (d): $q = \pi/14, \lambda = 1.5$. δ_S is the smoothness indicator defined in Eq. (22).

In Fig. 4, we present some examples for Lanczos coefficients, where $B_N \approx 2b_{N/2}$ is observed in cases where the original b_n grows in a smooth fashion (indicated by a small δ_S), as shown in [(a)(b)(d)]. In contrast, if the b_n is not smooth, its non-smooth structure carries over to B_N , leading to deviations between B_N and $2b_{N/2}$. This is similar to the finding in Fig. 1.

In Fig. 5 we show our estimation of $T_{\text{eq}}^{\text{rc}}$ for varying R for the cases [(a)-(d)] discussed in Fig. 4. Similar to

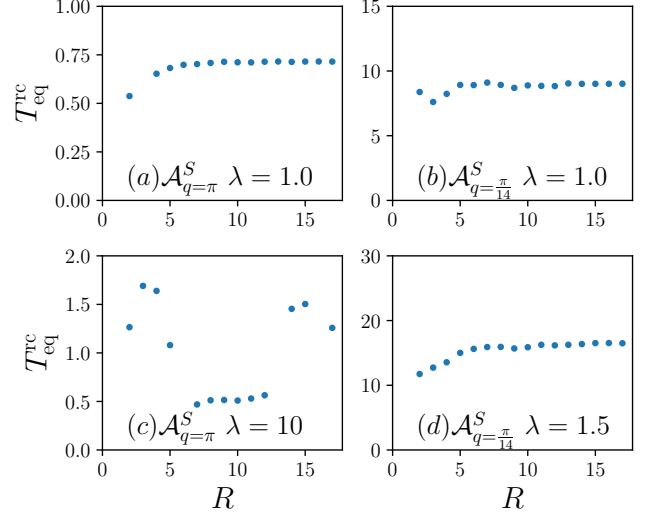


FIG. 5. Equilibration time $T_{\text{eq}}^{\text{rc}}$ (given in Eq. (16)) for different numbers R of included Lanczos coefficients, for the spin density wave operators in XXZ model. The results are shown for different λ and wave number q . (a): $q = \pi, \lambda = 1.0$; (b) $q = \pi/14, \lambda = 1.0$; (c): $q = \pi, \lambda = 10.0$ and (d): $q = \pi/14, \lambda = 1.5$.

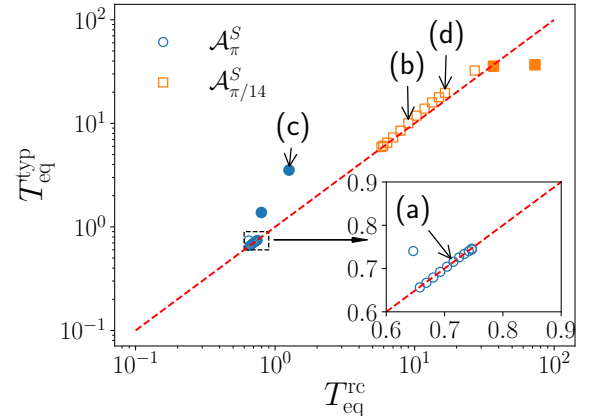


FIG. 6. Comparison between the equilibration time estimated using the recursion method $T_{\text{eq}}^{\text{rc}}$ (Eq. (16)), and that obtained from exact dynamics $T_{\text{eq}}^{\text{typ}}$ for the spin density wave operator \mathcal{A}_q^S in XXZ model with wave number $q = \pi, \pi/14$ and λ ($\lambda \in [0.5, 10.0]$). Open (solid) dots indicates results for $\delta_S < 0.2$ ($\delta_S \geq 0.2$). Here we choose $R = n_{\max}$. The inset shows a zoomed-in region for better distinguishability of the results.

the observables shown in Fig. 2, if Lanczos coefficients are smooth (as in the case of [(a)(b)(d)]), $T_{\text{eq}}^{\text{rc}}$ only varies slightly with respect to R , for $R \gtrsim 5$. In contrast, when the Lanczos coefficients exhibits significant fluctuations (in the case of (c)), the estimate $T_{\text{eq}}^{\text{rc}}$ does not converge, indicating that an accurate result for T_{eq} might not yet have been reached.

Furthermore, in Fig. 6 we benchmark the accuracy of

our estimate $T_{\text{eq}}^{\text{rc}}$ against the results from the direct simulations (using DQT) of the autocorrelation functions, denoted by $T_{\text{eq}}^{\text{typ}}$. In the DQT simulations, we consider system size $L = 28$. Good agreement between $T_{\text{eq}}^{\text{rc}}$ and $T_{\text{eq}}^{\text{typ}}$ is observed if δ_S is small (open dots), suggesting the high accuracy of our estimation. For large values of δ_S ($\delta_S \geq 0.2$), the deviation of $T_{\text{eq}}^{\text{rc}}$ from $T_{\text{eq}}^{\text{typ}}$ becomes noticeable (see, for example, point (c)).

To summarize, the additional numerics on the spin density wave operator in the Heisenberg model further suggest the result of the main text that, if the observable eventually shows smoothly growing Lanczos coefficients, a finite number of the former is sufficient for a reasonable estimate of the equilibration time.

SUPPLEMENTAL MATERIAL

Outline

Here we provide some analytical arguments that firstly, the concentration of the Krylov vector along the forefront of product space $\{|n_1\rangle\otimes|n_2\rangle\}$ is a self-consistent assumption, putting forward analytical evidence that for pertinent classes of Lanczos coefficients the evolution of the Krylov vector is particularly simple. Secondly, we translate the successive action of the Liouvillian into stochastic process. This enables us to infer statements on the structure of the Krylov vectors associated to the Lanczos coefficients B_n of the squared autocorrelation function $\mathcal{C}^2(t)$. Lastly, we bring together both of the above statements formulate an approximate relation between the Lanczos coefficients B_n of the squared dynamics and those of the original autocorrelation function, b_n .

Furthermore we provide 1): our estimate $T_{\text{eq}}^{\text{rc}}$ for the toy model with smooth Lanczos coefficients $b_n = \sqrt{n}$; 2): numerical results on the time integral of squared auto-correlation functions and 3): detailed derivations of Eq. (14) in the main text.

Concentration on forefront

Numerically we find that for pertinent Lanczos coefficients the Krylov vector for the squared dynamics, i.e. generated by $\mathcal{L} = \mathcal{L}_1 + \mathcal{L}_2$, for smooth Lanczos coefficients, is predominantly located at outmost counterdiagonal, see Fig. S1 for a first impression. We refer to this behaviour as *concentration on the forefront*. First, we introduce the labeling of states $|\alpha - \beta\rangle\otimes|\beta\rangle =: |\alpha, \beta\rangle$. Any state on the product space may be written as

$$|n\rangle = \sum_{\alpha, \beta=0} \Phi^n(\alpha, \beta) |\alpha, \beta\rangle. \quad (\text{S1})$$

We assume that $\Phi^n(\alpha, \beta) \approx 0$ for $\alpha \neq n$, i.e. that the vector is concentrated along the outmost counterdiagonal, the *forefront*. We check the self-consistency of this assumption, testing the appropriateness of the assumption in the first place. To this end, we formally rewrite action of the Liouvillian onto a state in two parts that raise (lower) in the value of α , i.e. propagate the state the next-higher (next-lower) counterdiagonal,

$$(\mathcal{L}_1 + \mathcal{L}_2)|n\rangle =: \mathcal{L}^-|n\rangle + \mathcal{L}^+|n\rangle, \quad (\text{S2})$$

$$(\alpha, \beta|\mathcal{L}^-|n\rangle = 0 \quad \text{for } \alpha \neq n-1, \quad (\text{S3})$$

$$(\alpha, \beta|\mathcal{L}^+|n\rangle = 0 \quad \text{for } \alpha \neq n+1. \quad (\text{S4})$$

The first Lanczos step finds

$$|n+1\rangle \propto \mathcal{L}^-|n\rangle + \mathcal{L}^+|n\rangle - [(n-1|\mathcal{L}^-|n\rangle + (n-1|\mathcal{L}^+|n\rangle)]|n-1\rangle.$$

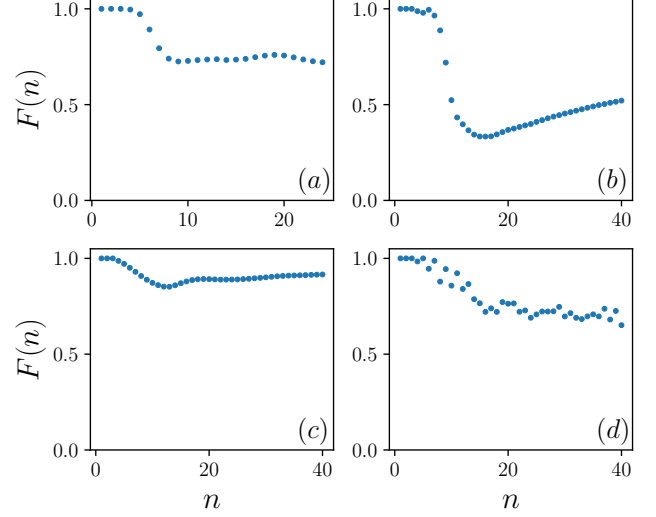


FIG. S1. *Concentration on the forefront:* $F(n)$ (Eq. (S12)) versus n for (a): Ising ladder, \mathcal{A}_Δ , $\lambda = 0.5$; (b): TFI, $\mathcal{A}_q(q = \pi/12)$, $\lambda = 0.5$; (c): TFI, $\mathcal{A}_q(q = \pi)$, $\lambda = 0.5$ and (d): TFI, $\mathcal{A}_q(q = \pi)$, $\lambda = 2.0$.

By virtue of Eq. (S4) the last term vanishes. Hence, to stay in line with the initial assumption we need to have $|n-1\rangle \propto \mathcal{L}^-|n\rangle$. Next, we turn to the second Lanczos step

$$|n+2\rangle \propto \mathcal{L}^- \mathcal{L}^+|n\rangle + (\mathcal{L}^+)^2|n\rangle - [(n|\mathcal{L}^- \mathcal{L}^+|n\rangle + (n|\mathcal{L}^+)^2|n\rangle)]|n\rangle. \quad (\text{S5})$$

As before, the last term vanishes due to Eq. (S4) and in order to find $|n+2\rangle \propto (\mathcal{L}^+)^2|n\rangle$ we need to have $\mathcal{L}^- \mathcal{L}^+|n\rangle \propto |n\rangle$. However, in contrast to the first Lanczos step, we may check this explicitly. Starting from a specific state $|\alpha, \beta\rangle$ the successive action of $\mathcal{L}^- \mathcal{L}^+$ involves 5 states and 4 Lanczos coefficients in total (one less resp. at the edges), as illustrated in Fig. S2. First, we define $\chi(\beta) := (\alpha+1, \beta|\mathcal{L}^+|n\rangle)$ as the amplitude of the *raised* state along the counterdiagonal $\alpha+1$. For this, in total 4 terms, originating from 3 different states along α contribute, see Fig. S2. Concretely, we have

$$\chi(\beta) = b_\beta \Phi^n(\alpha, \beta-1) + b_{\alpha-\beta+1} \Phi^n(\alpha, \beta), \quad (\text{S6})$$

$$\chi(\beta+1) = b_{\alpha-\beta} \Phi^n(\alpha, \beta+1) + b_{\beta+1} \Phi^n(\alpha, \beta). \quad (\text{S7})$$

Finally, the action of \mathcal{L}^- maps the state back to the counterdiagonal α . Denoting the overlap along this initial counterdiagonal by $\Psi(\alpha, \beta) := (\alpha, \beta|\mathcal{L}^- \mathcal{L}^+|n\rangle)$ we find

$$\Psi(\alpha, \beta) = -(b_{\beta+1} \chi(\beta+1) + b_{\alpha-\beta+1} \chi(\beta)) \quad (\text{S8})$$

$$= -(b_{\beta+1} b_{\alpha-\beta} \Phi^n(\alpha, \beta+1) + b_{\beta+1}^2 \Phi^n(\alpha, \beta)) \quad (\text{S9})$$

$$b_{\alpha-\beta+1} b_\beta \Phi^n(\alpha, \beta-1) + b_{\alpha-\beta+1}^2 \Phi^n(\alpha, \beta)).$$

If we further assume that the Lanczos coefficients change little, i.e. $b_n \approx b_{n+1}$, and that along some counterdiagonal α the profile is reasonably smooth, i.e. $\Phi^n(\alpha, \beta-1) \approx$

$\Phi^n(\alpha, \beta) \approx \Phi^n(\alpha, \beta + 1)$ Eq. (S9) simplifies to

$$\Psi(\alpha, \beta) \approx -(b_\beta + b_{\alpha-\beta})^2 \Phi^n(\alpha, \beta). \quad (\text{S10})$$

From this we can infer that if

$$b_\beta + b_{\alpha-\beta} = \text{const.} \quad \text{with respect to } \beta, \quad (\text{S11})$$

applies, $|n + 2| \propto (\mathcal{L}^+)^2 |n|$ may be fulfilled, hence concentration on the forefront may occur, see Fig. S3 for a check of Eq. (S11) for the physical cases (a)-(d). This also allows or a corresponding conclusion in an approximate sense. However, the condition (S11) is not only strictly fulfilled in the scenario of purely linear Lanczos coefficients b_n but also for Lanczos coefficients of the form $b_n = an + c$. It may also be approximately fulfilled for other sets of b_n . Revisiting Fig. S1, as well as Fig. 1 in the main text, we find that in the cases of suitably linear (and hence smooth) Lanczos coefficients (see cases (a)-(c)), i.e. cases that approximately fulfill the condition (S11), there is a concentration on the forefront. Conversely, in (d) the b_n deviate considerably from a linear form in the numerically accessible regime and the Krylov vector $|Q_n\rangle$ is hardly located at the forefront. We check

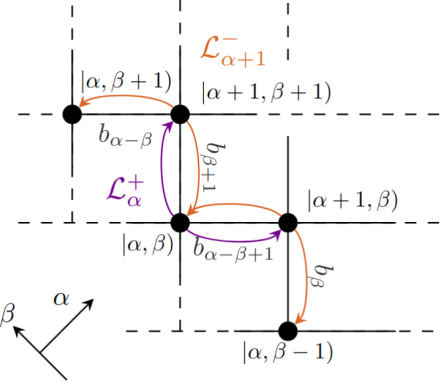


FIG. S2. Sketch of the action of $\mathcal{L}^- \mathcal{L}^+ |n\rangle$ on the product grid spanned by the Krylov state $\{|n_1\rangle \otimes |n_2\rangle\}$, “zoomed in” on the state $|\alpha, \beta\rangle$.

the assumption of concentration on the forefront by considering

$$F(n) = \sum_{\beta=0}^{\alpha} |\Phi^n(\alpha = n, \beta)|^2, \quad (\text{S12})$$

and the results are shown in Fig. S1.

Stochastic matrices

Our aim is to translate the repeated action of \mathcal{L}^+ into a stochastic process. Assuming an absolute concentration on the forefront, we consider a normalised state

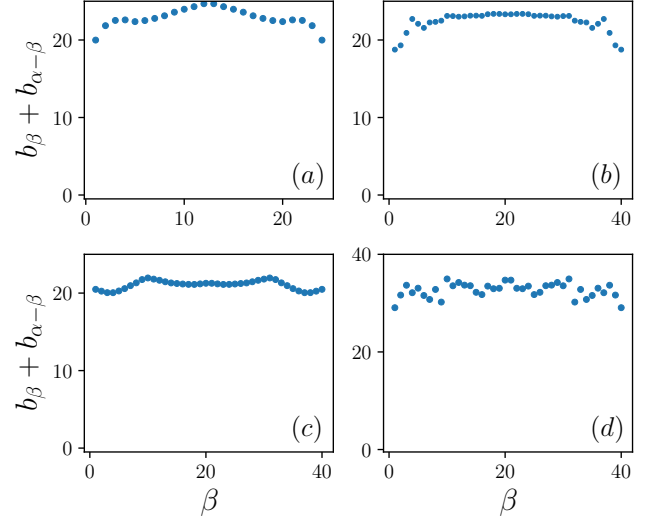


FIG. S3. $b_\beta + b_{\alpha-\beta}$ versus β for (a): Ising ladder, \mathcal{A}_Δ , $\lambda = 0.5$; (b): TFI, $\mathcal{A}_q(q = \pi/12)$, $\lambda = 0.5$; (c): TFI, $\mathcal{A}_q(q = \pi)$, $\lambda = 0.5$ and (d): TFI, $\mathcal{A}_q(q = \pi)$, $\lambda = 2.0$. Here we choose $\alpha = n_{\max}$.

$|Q_n\rangle = \sum_{k=0}^n p_k^n |n, k\rangle$ that is solely contained along the n^{th} counterdiagonal of the product space spanned by $\{|n_1\rangle \otimes |n_2\rangle\}$. Consequently, we focus on sets of Lanczos coefficients b_n that (locally) fulfill condition (S11), i.e. those that are (locally) of the form $b_n = an + c$. The operator \mathcal{L}_n^+ corresponds to the action of the Liouvillian propagating the amplitudes of a state from the counterdiagonal n to the next-highest counterdiagonal $n + 1$. Concretely,

$$\mathcal{L}_n^+ = \begin{pmatrix} b_n & 0 & 0 & \dots & 0 \\ b_1 & b_{n-1} & 0 & \dots & 0 \\ 0 & b_2 & \ddots & \ddots & 0 \\ \vdots & \ddots & \ddots & \ddots & \vdots \\ \vdots & \ddots & \ddots & b_{n-1} & b_1 \\ 0 & \dots & \dots & 0 & b_n \end{pmatrix}. \quad (\text{S13})$$

For better clarity, we turn to square matrices and consider operators of the form

$$\mathcal{M}_{n,d} = \left(\frac{1}{2(an/2+c)} \begin{bmatrix} \mathcal{L}_n^+ & \begin{matrix} v_0 \\ \vdots \\ v_n \end{matrix} \\ 0 & 0 \end{bmatrix} \right) \mathbb{1}_{d-n}, \quad (\text{S14})$$

where $v_0 = v_n = a + c$ and else $v_k = a$ for a and c from the linear form of the b_n . Here, several remarks are in order. First, the dimension-padding imposed by the identity matrix is done such that for some counterdiagonal d all matrices have the same dimension. For clarity of notation, we refrain from carrying the subscript explicit-

itly, i.e. $\mathcal{M}_n \hat{=} \mathcal{M}_{n,d}$. Secondly, the matrix \mathcal{M}_n is *doubly-stochastic*, i.e. $\sum_j (\mathcal{M}_n)_{jk} = \sum_k (\mathcal{M}_n)_{jk} = 1$. Further, we understand the occupation vectors as being padded into the proper ambient dimension, e.g. along the counterdiagonal n the occupation vector reads:

$$p^n = (p_0^n, p_1^n, \dots, p_n^n, \underbrace{0, \dots, 0}_{d-n}). \quad (\text{S15})$$

With this it becomes evident that when computing *new* occupation amplitudes of the state at the counterdiagonal $n+1$ we have

$$p^{n+1} = \mathcal{M}_{n+1} p^n, \quad (\text{S16})$$

$$= \Pi_{j=2}^{n+1} \mathcal{M}_j p^1 \quad (\text{S17})$$

for which neither for the dimensionality-padding constructions for \mathcal{L}_n^+ , \mathcal{M}_n or p^n enter. For better accessibility, we show in Fig. S4 the respective Markov chain for the transition from counterdiagonal $n = 2 \rightarrow 3$, i.e. the action of \mathcal{M}_2 .

For every counterdiagonal n we consider the quantity:

$$H^n = - \sum_j p_j^n \ln \left(\frac{p_j^n}{q_j^n} \right), \quad (\text{S18})$$

where the $\{q_i^n\}$ denote equilibrium probabilities of the stochastic process generated by the \mathcal{M}_n and the p_j^n label the entries of the occupation vector p^n , i.e. the actual probabilities at the position j at the iteration n . By virtue of Ref. [36] the quantity defined by Eq. (S18) is monotonous with respect to n and hence identifies the direction of the approach to equilibrium of the stochastic process imposed by \mathcal{L} .

For each \mathcal{M}_n we have $q_j^n \equiv 1/d$ which follows from the double stochasticity of the \mathcal{M}_n , hence

$$H^n = - \sum_j p_j^n (\ln p_j^n - \ln d). \quad (\text{S19})$$

constitutes a monotonous function in n . This quantity (up to the constant addend $-\ln d$) may be interpreted as the (increasing) Shannon entropy of the stochastic process along n . Consequently, the growing entropy implies the successive *smoothening* of the occupation vectors p_j^n along n and with respect to j , i.e. the distribution of the Krylov states $|Q_n\rangle$ gets successively wider. Note that in the setting of the preceding subsection this finding translates to an increasing applicability of the assumption $\Phi^n(\alpha, \beta - 1) \approx \Phi^n(\alpha, \beta) \approx \Phi^n(\alpha, \beta + 1)$.

For Lanczos coefficients of operators in real quantum many-body systems, the picture is clearly more intricate than in the scenario of linear Lanczos coefficients above, as the matrices \mathcal{M}_n are generally not fully *doubly stochastic*. However, also in the physical cases (b) and (c) studied throughout this paper we find that the corresponding Lanczos coefficients b_n *locally* fulfill condition (S11), see

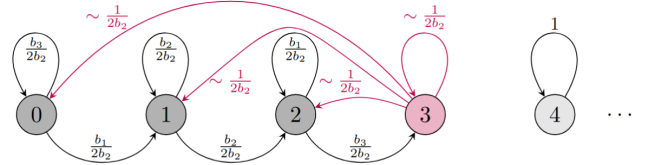


FIG. S4. Markov chain of the stochastic process corresponding to the action of \mathcal{M}_2 . The input here is given by the three entries p_0^2, p_1^2, p_2^2 of the occupation vector on the second counterdiagonal, indicated by the gray circles “0”, “1”, “2”. The entry at “3” is initially zero, i.e. $p_3^2 = 0$, hence the contribution to the other states indicated by the arrow $\sim \frac{1}{2b_2}$ have no weight in the stochastic process. However, there are non-zero rate towards “3”, such that $p_3^3 \neq 0$ for the subsequent step of the process, i.e. \mathcal{M}_3 (not shown).

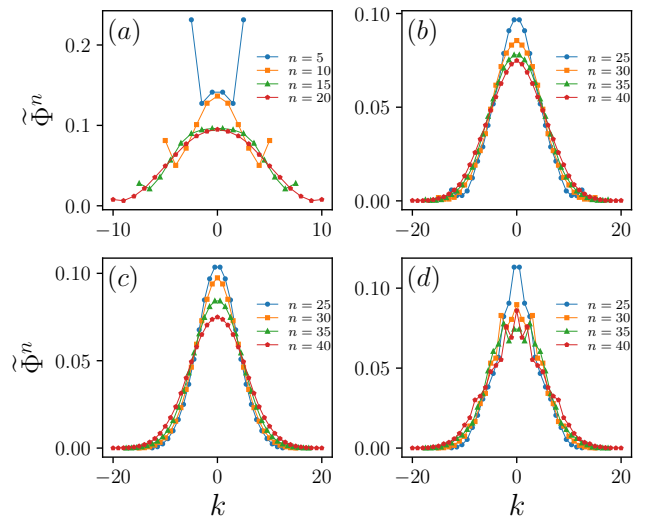


FIG. S5. *Distribution along the forefront*: Spread of the normalized coefficients $\tilde{\Phi}^n(\alpha = n, k) \propto p_k^n$ at several counterdiagonals n for (a): Ising ladder, \mathcal{A}_Δ , $\lambda = 0.5$; (b): TFI, $\mathcal{A}_q(q = \pi/12)$, $\lambda = 0.5$; (c): TFI, $\mathcal{A}_q(q = \pi)$, $\lambda = 0.5$ and (d): TFI, $\mathcal{A}_q(q = \pi)$, $\lambda = 2.0$.

Fig. S3, whereas for case (d) the condition is violated. Here we leave out case (a), as in this scenario the accessible number of Lanczos coefficients is too low for an adequate analysis. However, the plateau that becomes visible in the bulk, suggests that eventually also in this case condition (S11) will be fulfilled.

In Fig. S5 we examine the distribution of the Krylov vectors $|Q_n\rangle$ at several forefronts n , i.e. the spread of the coefficients $\Phi^n(\alpha = n, k)$ along k . Relating to the language of occupation vectors and amplitudes, this is equivalent to the spreading of the occupation amplitudes p_k^n along k for various n . We find that in the cases of smooth Lanczos coefficients, that (locally) comply with (S11), the occupation amplitudes spread out, reminiscent of a diffusive process (here (a)-(c)). Again the case (d)

stands out as the profile does not smoothen out, contrary to the other scenarios in which consequently the idea of a growing (Shannon) entropy, see Eq. (S19), becomes tangible.

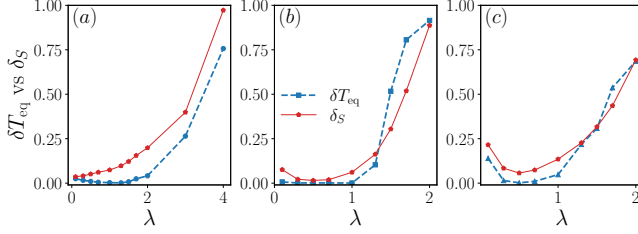


FIG. S6. $\delta T_{\text{eq}} = \frac{|T_{\text{eq}}^{\text{rc}} - T_{\text{eq}}^{\text{typ}}|}{T_{\text{eq}}^{\text{typ}}}$ (solid line) and smoothness δ_S (dashed line) versus λ for operators (a): Ising ladder \mathcal{A}_Δ , (b) TFI: \mathcal{A}_π and (c) $\mathcal{A}_{\pi/12}$.

Approximation formula

Consider the amplification of a normalized vector $|Q_n\rangle$ under the action of \mathcal{L}_n^+ . Assuming a full concentration on the forefront, the j^{th} entry of the vector $|\tilde{Q}_{n+1}\rangle := \mathcal{L}_n^+|Q_n\rangle$ gets amplified by a factor $b_{n-j} + b_j$. Note that for the case of $b_k = ak + c$ we get

$$b_{n-j} + b_j = an + 2c = 2b_{\frac{n}{2}} \quad (\text{S20})$$

For the Lanczos coefficient related to the this new Krylov vector we have

$$B_{n+1} = \sqrt{(\tilde{Q}_{n+1}|\tilde{Q}_{n+1})}. \quad (\text{S21})$$

If we assume additionally that the vector $|Q_n\rangle$ is spread out sufficiently even (see preceding section), we may infer an approximation of the B_n by

$$B_n \approx 2b_{\frac{n}{2}}. \quad (\text{S22})$$

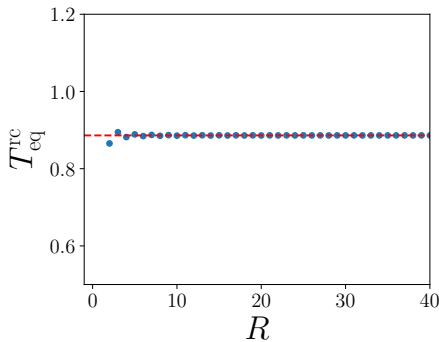


FIG. S7. $T_{\text{eq}}^{\text{rc}}$ as a function of R (starting point of the linear continuation of B_N), for the toy model $b_n = \sqrt{n}$. The dashed line indicates the analytical prediction $T_{\text{eq}} = \frac{\sqrt{\pi}}{2}$.

Benchmark cases

One of the few examples of analytically known connections between autocorrelation functions and Lanczos coefficients is given by

$$C(t) = \exp\left(-\frac{t^2}{2}\right) \longleftrightarrow b_n = \sqrt{n}. \quad (\text{S23})$$

This case is especially interesting as it also allows to infer the Lanczos coefficients for the squared autocorrelation function, which here also turns out to be a Gaussian (with different variance),

$$C^2(t) = \exp(-t^2) \longleftrightarrow B_n = \sqrt{2n}. \quad (\text{S24})$$

We find that in this case $2b_{n/2} = \sqrt{2n} = B_n$, and hence that our approximation formula (S22), derived on the basis of a stochastic process, is exact.

For purely linear Lanczos coefficients $b_n = \alpha n$ the Lanczos algorithm on the product space $\{|n_1\rangle \otimes |n_2\rangle\}$ is particularly simple as the contributions by \mathcal{L}^- vanish in the orthogonalization and the Krylov vector is hence fully located at the forefront. For this special case the distribution along the counterdiagonal is constant, as the number of "paths" to each site on the counterdiagonal and the corresponding "weight" given by the Lanczos coefficients cancel,

$$|Q_n\rangle = \frac{1}{\sqrt{n+1}} \sum_{k=0}^n |n-k\rangle |k\rangle. \quad (\text{S25})$$

From this the Lanczos coefficients of the squared autocorrelation function follow as

$$B_n = \alpha \sqrt{n(n+1)}. \quad (\text{S26})$$

In this scenario, for large $n \gg 1$ we find linear growth and therefore an approximate agreement with Eq. (S22). In fact, the case of entirely linear Lanczos coefficients is special as in this case the spread of the Krylov vectors $|Q_n\rangle$ is uniform. When computing the Lanczos coefficient B_n as in Eq. (S21) we must take into account, that the dimension of the $|Q_{n-1}\rangle$ is n whereas $|Q_n\rangle = \mathcal{L}_n^+|Q_{n-1}\rangle / \|\cdot\|$ is $n+1$. With this we find

$$B_n = 2b_{n/2} \sqrt{\frac{n+1}{n}} = \alpha \sqrt{n(n+1)}. \quad (\text{S27})$$

However, in general the influence from the growing dimension is negligible, since the spread of the Krylov vectors falls off towards the edges, see Fig. S5. Therefore we generally expect the simple approximation (S22) to hold well.

Derivation of Eq. (14) in the main text

In this section, we show the detailed derivation of Eq. (14) in the main text. To this end, we insert

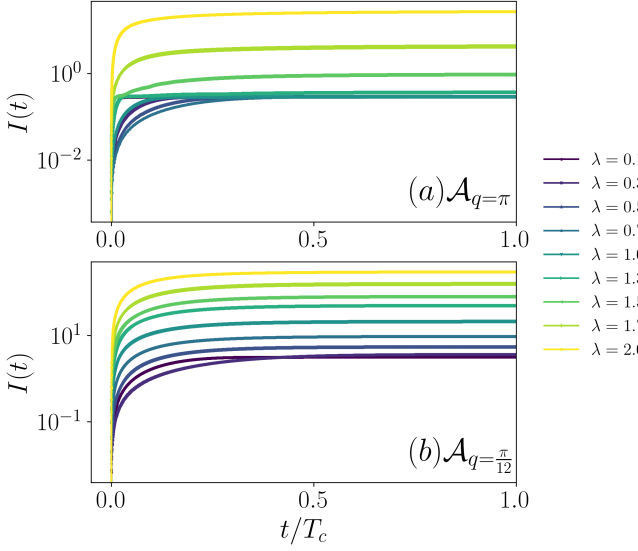


FIG. S8. Time integral of the squared autocorrelation function: $I(t)$ (defined in Eq. (S34)) versus t/T_c for (a): $\mathcal{A}_{q=\pi}$ and (b): $\mathcal{A}_{q=\frac{\pi}{12}}$ in the tilted field Ising model for different λ . The system size is $L = 24$.

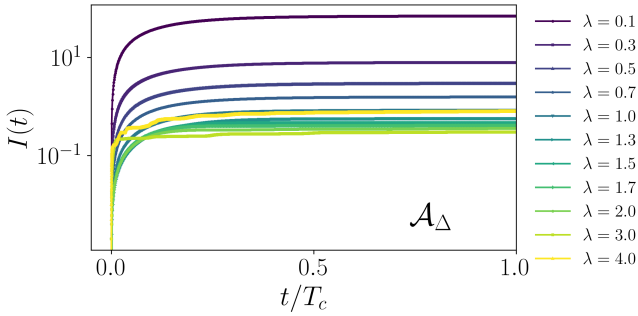


FIG. S9. Similar to Fig. S8, but for \mathcal{A}_Δ in the Ising ladder. The system size is $L = 24$.

$B_N(N > R) = \alpha N + \beta$ to Eq. (15). This leads to

$$\begin{aligned} p_R &= \prod_{k=1}^{\infty} \frac{(B_{2k+R-1})^2}{B_{2k+R} b_{2k-2+R}} \\ &= \prod_{k=1}^{\infty} \frac{(\alpha(2k+R-1) + \beta)^2}{(\alpha(2k+R) + \beta)(\alpha(2k-2+R) + \beta)} \\ &= \prod_{k=1}^{\infty} \frac{\left(k + \frac{\alpha R + \beta}{2\alpha} - \frac{1}{2}\right)^2}{\left(k + \frac{\alpha R + \beta}{2\alpha}\right)\left(k + \frac{\alpha R + \beta}{2\alpha} - 1\right)}. \end{aligned} \quad (\text{S28})$$

Making use of the following expression of Gamma function

$$\Gamma(z+1) = \prod_{k=1}^{\infty} \left[\frac{1}{1 + \frac{z}{k}} \left(1 + \frac{1}{k} \right)^z \right], \quad (\text{S29})$$

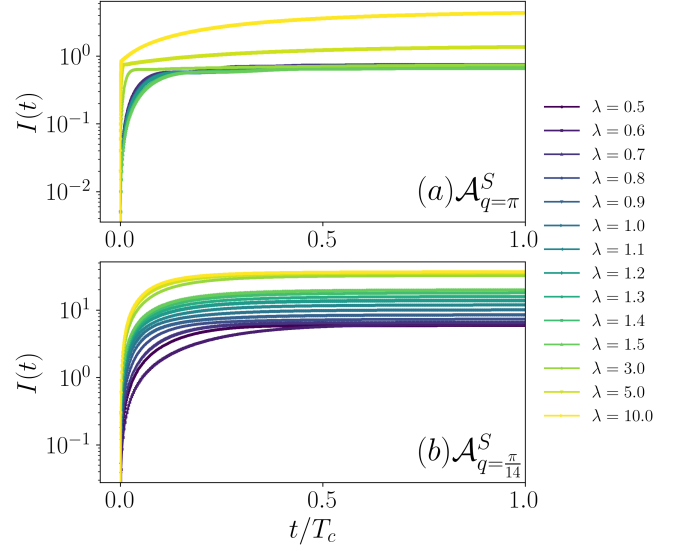


FIG. S10. Similar to Fig. S8, but for (a): $\mathcal{A}_{q=\pi}^S$ and (b): $\mathcal{A}_{q=\frac{\pi}{14}}^S$ in the XXZ model. The system size is $L = 28$.

it is easy to get

$$\frac{\Gamma(z - a + 1)\Gamma(z + a + 1)}{\Gamma^2(z + 1)} = \prod_{k=1}^{\infty} \frac{(k + z)^2}{(k + z - a)(k + z + a)}. \quad (\text{S30})$$

Comparing Eq. (S30) with Eq. (S28), and setting $z = \frac{R}{2} + \frac{\beta}{2\alpha} - \frac{1}{2}$, $a = \frac{1}{2}$, one has

$$p_R = \frac{\Gamma(\frac{R}{2} + \frac{\beta}{2\alpha})\Gamma(\frac{R}{2} + \frac{\beta}{2\alpha} + 1)}{\Gamma^2(\frac{R}{2} + \frac{\beta}{2\alpha} + \frac{1}{2})}, \quad (\text{S31})$$

which is the result of Eq. (14).

I. MORE DETAILS ON THE CALCULATION OF $T_{\text{eq}}^{\text{typ}}$

$T_{\text{eq}}^{\text{typ}}$ is defined as

$$T_{\text{eq}}^{\text{typ}} := \int_0^{T_c} |\mathcal{C}_{\text{typ}}(t)|^2 dt, \quad (\text{S32})$$

where $\mathcal{C}_{\text{typ}}(t)$ represents the autocorrelation function calculated via dynamical quantum typicality [32] (DQT):

$$\mathcal{C}_{\text{typ}}(t) = \langle \psi | \mathcal{O}(t) \mathcal{O} | \psi \rangle. \quad (\text{S33})$$

The state $|\psi\rangle$ is a normalized Haar-random state, the real and imaginary part of which are Gaussian random numbers. T_c indicates the cutoff time, which is determined by the time after which $|\mathcal{C}_{\text{typ}}(t)|^2 \leq 0.001$ for all computable times $t \geq T_c$. To further check whether $T_{\text{eq}}^{\text{typ}}$ is insensitive to the cutoff time T_c , in Figs. S8, S9 and S10,

we plot

$$I(t) = \int_0^t |\mathcal{C}_{\text{typ}}(s)|^2 ds \quad (\text{S34})$$

in the tilted field Ising model, Ising ladder and XXZ model and various of observables. Note that $T_{\text{eq}}^{\text{typ}} = I(t =$

T_c). It is clear from the figures that, for all cases considered, $I(t)$ approximately saturate at $t < T_c$. This implies that $T_{\text{eq}}^{\text{typ}}$ is indeed insensitive to the cutoff time T_c .